Observation of Simultaneous Axial and Transverse Classical Heat Transport in a Magnetized Plasma

A. T. Burke, J. E. Maggs and G. J. Morales

Department of Physics and Astronomy

University of California, Los Angeles, CA 90095

ABSTRACT

The transport of heat deposited by a small low voltage electron beam in a strongly magnetized plasma is studied for a time interval in excess of two thousand ion gyro-periods. Electron temperatures are observed to evolve along and across the magnetic field at the classically predicted rates up to times approaching one thousand gyro-periods. At later times the onset of low frequency fluctuations (below one tenth the ion gyrofrequency) coincides with departures from classical behavior.

PACS: 52.25 Fi, 52.50 Gj, 52.35 Qz

The theoretical foundations of heat transport due to Coulomb collisions (i.e., classical transport) in strongly magnetized plasmas (i.e., electron gyrofrequency much larger than the Coulomb collision frequency, $\Omega_e >> \nu_{ie}$) have been known[1,2,3] for nearly half a century. However, this intrinsically anisotropic phenomenon has been extremely difficult to observe in the laboratory for both fundamental reasons and lack of suitable experimental facilities. It is quite common for heat transport experiments to yield transport rates that are enhanced by orders of magnitude over the classical values (i.e., so-called anomalous transport); the extreme measure of anomaly for cross-field transport being the Bohm-diffusion coefficient. In this letter we report measurements of electron heat transport from a carefully chosen experimental arrangement using the Large Plasma Device[4] (LAPD) at UCLA that conclusively demonstrates the two-dimensional (i.e., simultaneous transport along and across the confining magnetic field) pattern characteristic of the classical theory. It is also shown that classical transport proceeds until the spontaneous growth of fluctuations overwhelms the effects of Coulomb collisions.

It should be emphasized that the past decade has seen the development of increasingly sophisticated basic plasma experiments probing the nature of classical transport. Noteworthy among these are measurements of the effective cross-field thermal conductivity[5], determination of velocity-space transport[6], and test particle transport in non-neutral plasmas[7].

The classical electron thermal conductivity in the axial direction (along the confining magnetic field, B_0) is given[2] by $\kappa_{||} = (3.16) n_e T_e \tau_e / m_e$, and, in the transverse direction, by $\kappa_{\perp} = (1.47) \kappa_{||} (\Omega_e \tau_e)^{-2}$, where n_e is the electron plasma density, T_e the electron temperature (in electron-volts), m_e the electron mass and $\tau_e = (3.44 \times 10^5) T_e^{3/2} / (n_e \lambda)$, with λ the usual Coulomb logarithm (λ = 12.0 for the results reported here). The unique features of classical transport are that $\kappa_{||} \propto T_e^{5/2}$ while $\kappa_{\perp} \propto B_0^{-2} T_e^{-1/2}$, which results in a large degree of anisotropy that typically prevents a clear study of the three-dimensional propagation of heat pulses in magnetized plasmas. To overcome the large disparity in the axial and transverse rates one must consider very long systems (of length L) and apply heat sources of small transverse extent (of radius a). When the condition $(a/L) < 1.72 (\Omega_e \tau_e)^{-1}$ is satisfied, the rate of radial energy loss across the surface of a heated filament exceeds the rate of axial loss through the ends, and the anisotropic nature of the heat transport can be probed. Meeting this condition is the essence of the present study.

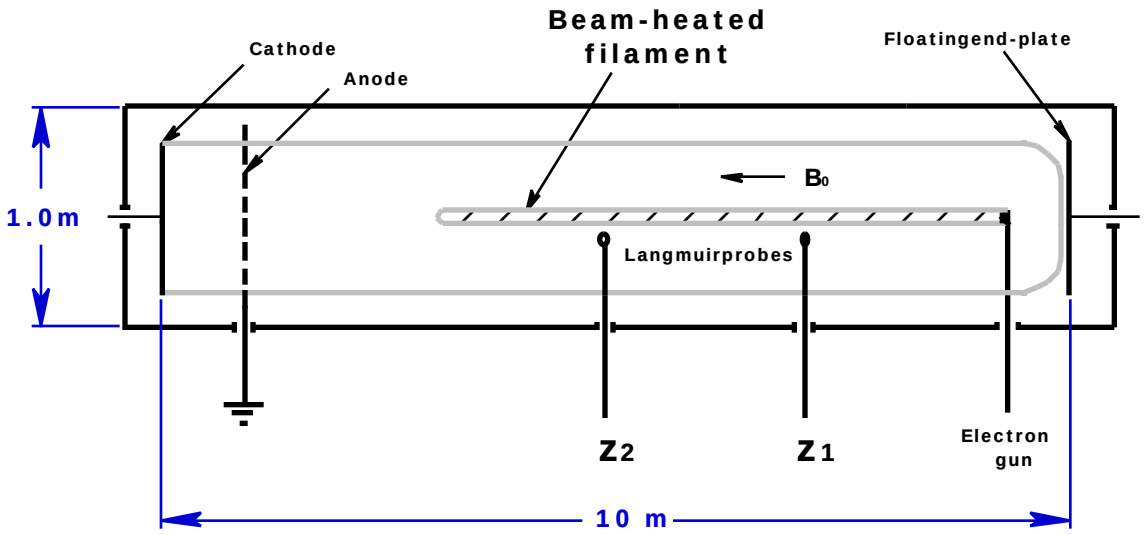

Fig. 1. Schematic of the experimental set up. A small (3 mm diameter) electron beam source is located near the end of the device away from the cathode. A low voltage beam (20 V) produces a heat source which creates a field-aligned temperature plume. Planes of Langmuir probe data are taken at axial locations z_1 (285 cm) and z_2 (410 cm) far away from the heat source.

The experimental setup is illustrated in Fig. 1. A large 40 cm diameter background plasma is generated by electrons emitted from a heated, Barium-Oxide coated cathode and subsequently accelerated (to about 50 V) by a semi-transparent grid anode located 60 cm from the cathode. The accelerated electrons drift into a 9.4 m long vacuum chamber and strike neutral Helium gas at a fill pressure of $1.\times10^{-4}$ Torr to produce a plasma with a greater than 75% degree of ionization with measured densities of $1.-4.\times10^{12}$, $T_e = 6-8$ eV and ion temperature $T_i = 1$ eV, at $B_0 = 1$ kG. For this field strength the ions are so strongly magnetized that, for the present purposes, the plasma column can be considered infinite in radial extent.

The heat transport studies reported here are performed in the so-called afterglow phase of the plasma, i.e., after the discharge voltage pulse is terminated. In the afterglow plasma T_e decays rapidly (on a time scale of 100 μs) due to classical axial transport (radial transport is negligible because a/L is large) to the ends of the device and cooling due to energy transfer to the ions (an important process for $T_e < 1.5$ eV). The plasma density, however, decays slowly (on a time scale of 2 ms) due to ambipolar flow at the sound speed. The heat source generator consists of a small electron beam 3 mm in diameter (comparable to the electron skin depth) produced by biasing a heated, single crystal of Lanthanum-hexaboride to 20 V negative relative to the anode. The beam-generating crystal is located 75 cm from the end of the plasma column (i.e., 9.25 meters from the cathode). For the low beam voltages used in these experiments the extra ionization produced by the beam electrons is negligible. The beam electrons are slowed by the background plasma, thus depositing their energy, in a distance of about 1 m (beyond that there is no evidence for beam electrons in the electron velocity distribution). The beam therefore produces a heat source a few millimeters in diameter and about a meter in length. A beam current of 200 mA is used resulting in a heat source strength, Q_b, of approximately $0.2\ W/cm^3$.

Electron temperature measurements are taken at axial locations significantly larger than the axial extent of the heat source. As indicated in

Fig. 1, Langmuir probes are inserted at two locations, z_1 (located 285 cm from the beam source) and z_2 (410 cm from the beam source). The probes are scanned in the plane perpendicular to B_0 over rectangular grids with 1.5 mm spacing between grid points. At each spatial location, the temporal behavior of the ion saturation current is obtained for twenty separate pulses of the discharge plasma. Ion saturation current, I_{sat}, is converted to electron temperature by assuming $I_{sat} \quad n_e T_e^{1/2}$. The electron density is obtained by using the phase shift[8] of a 56 GHz interferometer located at z = 200 cm to calibrate a density profile of the plasma column obtained from Langmuir probe measurements. The magnitude of the electron temperature is calibrated using values obtained from Langmuir probe I-V traces taken just before the beam is turned on. The electron temperature obtained using this technique agrees very well with temperature measurements obtained at 80 μs intervals with Langmuir probe voltage sweeps. Also the voltage sweeps from the Langmuir probe confirm that the velocity distribution of the electrons is Maxwellian.

In order to obtain a meaningful quantitative test of the predictions of classical transport theory we have developed a two-dimensional, nonlinear, time evolution transport code using standard techniques (the alternating-direction implicit method[9]). The code incorporates realistic boundary conditions, including the interception of a finite amount of heat by the support structure of

the beam injector. The code includes only heat conduction terms, heat convection is assumed to be negligible. The equation solved is

$$\frac{3}{2} n_e \frac{\partial T_e}{\partial t} = \frac{1}{r} \frac{\partial}{\partial r} \left[r \kappa_{\perp} \frac{\partial T_e}{\partial r} \right] + \frac{\partial}{\partial z} \left[\kappa_{\parallel} \frac{\partial T_e}{\partial z} \right] - 3 \frac{m_e}{m_i} \frac{n_e}{\tau_e} \left(T_e - T_i \right) + Q_b , \quad (1)$$

together with the local ion temperature equation

$$\frac{3}{2} \frac{\partial T_i}{\partial t} = \frac{3}{\tau_e} \frac{m_e}{m_i} \left(T_e - T_i \right) - 3 \left(T_i - T_0 \right) n_0 \sigma_{i0} \left[\frac{T_i}{m_i} \right]^{1/2} , \quad (2)$$

where (r, z) refer to the radial and axial coordinates, m_i is the ion mass, with n_0 the neutral density and σ_{i0} the collision cross section of neutral Helium.

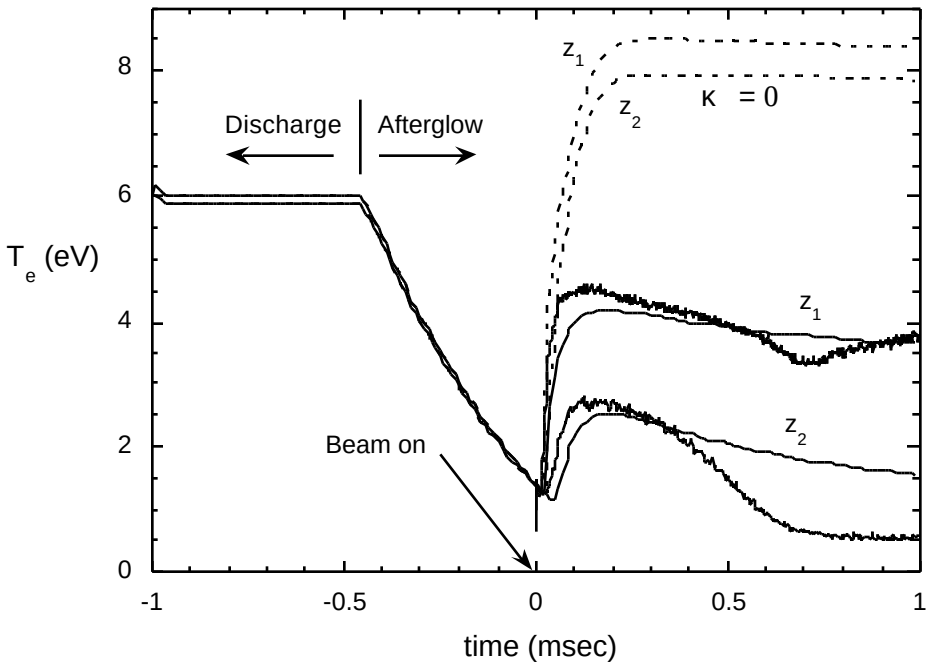

Fig. 2. Measured temporal behavior of electron temperature compared to predicted behavior at axial locations z_1 and z_2. The beam is turned on 0.5 ms after the discharge pulse is terminated and the electron temperature in the center of the beam source is observed to rise at both locations (noisy curves beginning at t = 0). The conduction of heat due to Coulomb collisions using classical coefficients predicts the observed behavior (smooth curves beginning at t = -1.0 ms). Radial transport is essential. The temperature plume would be much longer and the temperature much higher if the radial heat conduction coefficient were zero ($\kappa = 0$, the broken curves).

The time evolution of the electron temperature at a radial location corresponding to the center of the beam is shown in Fig. 2. The smooth solid curves beginning at t = -1 ms are the numerical solutions to Eqs. (1) and (2) at the two axial locations z_1 and z_2. The predicted temperature behavior extends from during the discharge, just before termination of the discharge voltage pulse, to 1 ms after the beam is turned on. The beam is turned on 0.5 ms after

termination of the discharge pulse. For this case the plasma density is taken to remain constant at $2.25 \times 10^{12}\,\mathrm{cm}^{-3}$. This assumption simplifies the comparison of theory to experiment by removing one variable from the theory and is a good approximation for the relatively short time interval (1ms) examined in this case. The measured variation in plasma density is used in the theory when comparing the temperature evolution over a longer time interval. The two theoretical curves are to be compared to the measured evolution of the electron temperature represented by the noisy solid curves beginning at t = 0 (these traces are averaged over twenty plasma pulses). The broken curves beginning near t = 0 correspond to the theoretical prediction neglecting the effect of radial transport (i.e., setting $\kappa = 0$ in Eq. (1)). It is immediately evident that for this system the classical theory predicts that radial transport plays a major role in determining the electron temperatures achieved far from the source. The observed rise times and peak temperatures achieved at each axial location are essentially the same as predicted by theory. The main discrepancies between theory and observation are the time after beam turn-on at which the temperature rise begins and the decay of the temperature at axial location z_2 after 0.4 ms. Both of these observed features can be reproduced in the theory by adjusting model parameters, such as the source size (radial and axial extent) and strength. However, since we do not have a detailed knowledge of the source, we have chosen not to arbitrarily adjust model parameters to improve the fit between theory and observation. The fact

the theoretical and experimental curves do not overlap perfectly in Fig. 2 should not be misinterpreted as a deviation from classical behavior. Instead, the deviations reflect uncertainty in some of the experimental elements and are a fair assessment of the degree of experimental control we have in this 3-dimensional classical transport experiment. Given the strong nonlinearity of the thermal conductivities in classical transport the degree of agreement between experiment and observation is remarkable.

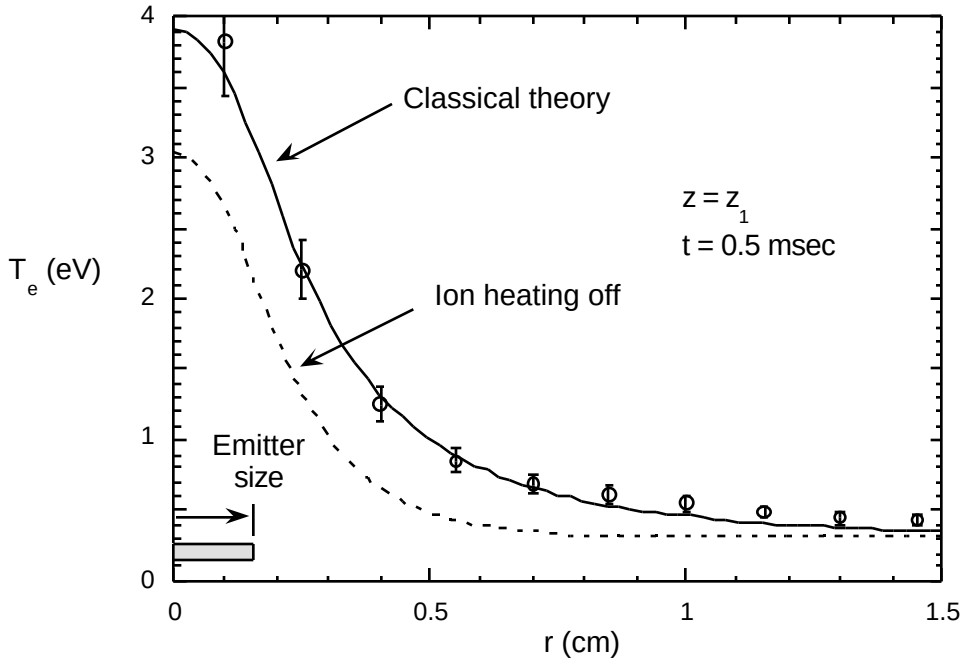

Fig. 3. Comparison of measured radial temperature profile (open circles) to the classical prediction (smooth continuous curve) at axial location z_1, 0.5 ms after beam turn on. The dashed curve is the predicted profile when the ion heating source in Eq. (2) is zero.

As a further illustration of the applicability of classical transport theory to these observations Fig. 3 shows the measured and predicted radial profiles at axial location z_1 at a time 0.5 ms after beam turn on. The solid curve is the theoretical prediction and the circles indicate the measured temperature. The agreement is very good. These observations also illustrate the importance of including ions in the heat balance equations. If ion heating by electrons is not included in the theoretical model the predicted profile is given by the dashed curve.

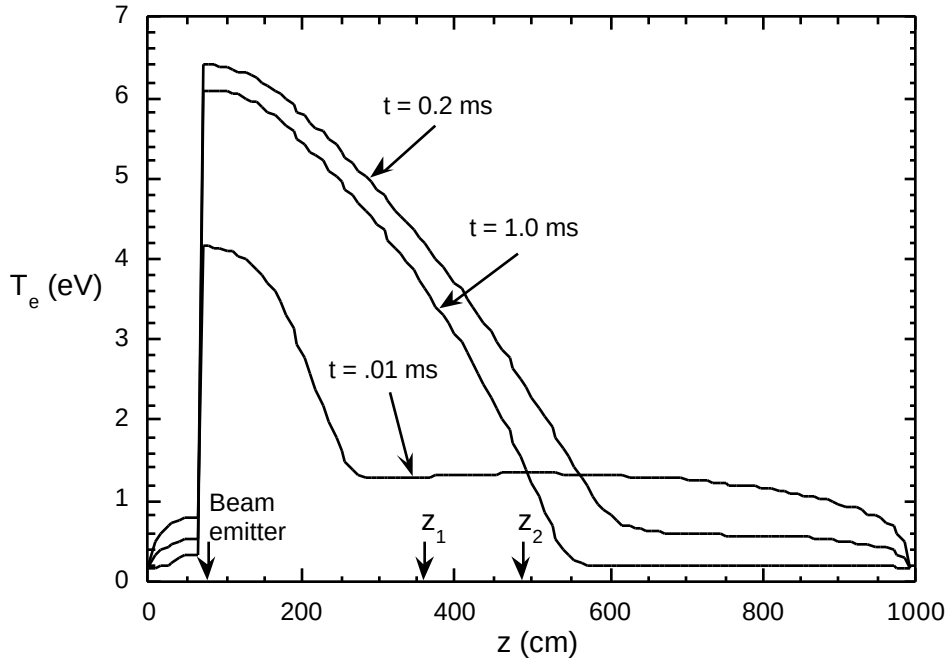

Fig. 4. Overview of the theoretically predicted spatial and temporal behavior of the temperature plume. The beam is turned on when the electrons in the background plasma are still warm (about 1.5 eV) and the temperature plume grows axially reaching a maximum extent at about 0.2 ms after beam turn on. The plume then contracts reaching a balance

between radial and axial transport after about 1.0 ms. The insert shows contours of electron temperature in 0.5 eV intervals beginning at 0.5 eV (the radial direction is magnified by a factor of 400).

Figure 4 illustrates the temporal evolution of the axial temperature profile as predicted by the two-dimensional classical heat transport code. Also shown as an insert is the spatial distribution (r, z) of the temperature at a fixed time (1.0 ms after beam turn-on). This figure illustrates a rather non-intuitive behavior for the heat pulse. Early in time (the curve marked .01 ms) the temperature increases rapidly in the vicinity of the heat source location (75 cm < z < 175 cm). Strong axial conduction leads to an elongated temperature plume extending as far as z = 600 cm at t = 0.2 ms. However, as the shape of the plume evolves and the value of a/L decreases, radial transport becomes dominant and leads to a contraction of the temperature plume which is manifested as a cooling of the initially observed temperature at large axial distances. This cooling effect due to axial contraction is very prominent in the observed temperature behavior at axial location z_2 as shown in Fig. 2. The insert in Fig. 4 depicts the predicted spatial distribution of the temperature. Contours of constant temperature are shown at intervals of 0.5 eV, starting at $T_e = 0.5$ eV. The radial distance is magnified by a factor of 400 for clarity. The effect of heat absorption by the support structure ($r \leq 0.5$ cm) of the beam injector on the temperature distribution is clearly apparent.

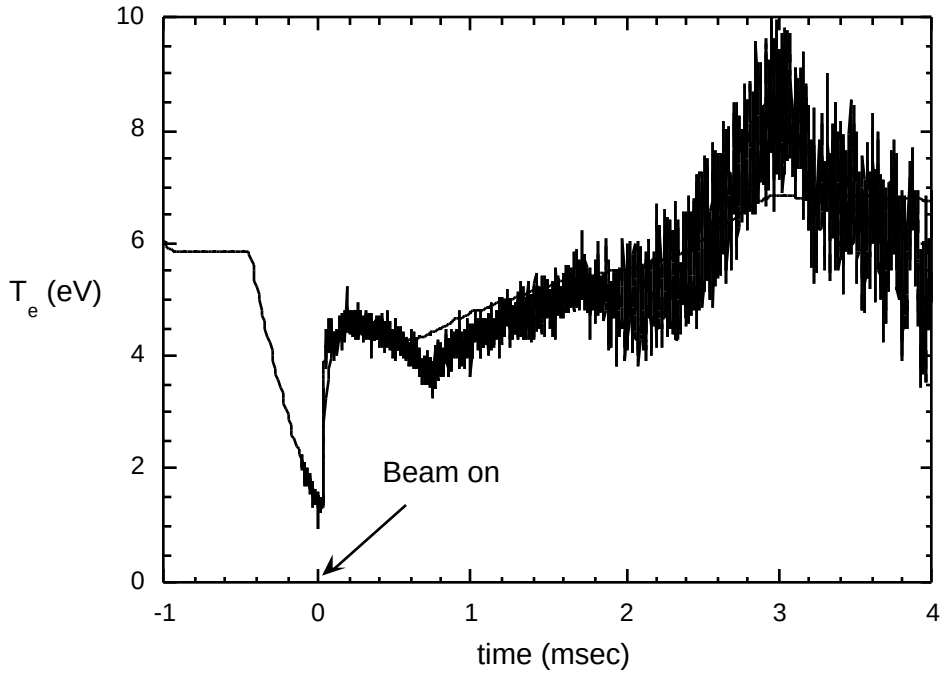

Fig. 5. The observed temperature in the center of the heated region (noisy curve) is compared to the classical prediction (smooth curve) for an extended time interval. The predicted curve includes the measured variation in plasma density. Classical conduction is observed for the first 2.0 ms, after which fluctuations with frequencies about 0.1 f_{ci} spontaneously grow. After onset of these fluctuations the electron temperature grows faster than predicted by classical theory. At about 3 ms low frequency fluctuations (about .02 f_{ci}) occur and lead to a rapid drop in the electron temperature.

Classical heat transport does not continue on long time scales, for a fixed heat source, as shown in Fig. 5. The observed time evolution of the electron temperature is shown (noisy curve) for an interval of 4 ms after beam turn-on at axial location z_1 at the center of the beam (r = 0). Also shown is the behavior of the temperature as predicted by classical transport theory (smooth curve). Here, as opposed to Fig. 2, we have included the effects of changing plasma density in the

theoretical predictions. Oscillations in the ion saturation current at a frequency of about 0.1 f_{ci} are observed to spontaneously develop about 2 ms after beam turn-on. These fluctuations may well represent variations in density rather than electron temperature, but under the assumptions employed here in converting ion saturation current to electron temperature they show up as temperature fluctuations. In addition, large amplitude fluctuations at lower frequency (about .02 f_{ci}) appear at around 3 ms after beam turn-on. The higher frequency modes are spatially located mainly in the radial gradient regions of the temperature plume and are akin to drift-Alfvén waves[10] while the low frequency modes are confined to the central region of the plume and resemble ion acoustic waves. Details of the interesting wave activity and nonlinear behavior require a separate study. Nonetheless, it is evident that, after the onset of fluctuations, significant departures from predicted classical behavior develop. First, after onset of the high frequency fluctuations, the central temperature of the plume rises faster than classical predictions and then rapidly decreases after onset of the low frequency fluctuations.

In summary, a carefully designed experiment has been able to demonstrate the simultaneous development of axial and transverse electron heat transport due to Coulomb collisions in a strongly magnetized plasma. A two dimensional transport code using classical thermal conductivities and including ion dynamics gives excellent agreement with the initial observed temporal and spatial development of the electron temperature. Over long times, low and high

frequency fluctuations develop spontaneously in various regions of the temperature plume leading to departures from classical heat transport behavior.

Acknowledgments: This work is part of the Ph.D. requirements for A. T. Burke at the University of California, San Diego. Research performed by A. T. Burke was sponsored by ONR, that of J. E. Maggs by ONR and NSF, and G. J. Morales by DOE and ONR.

References

[1] L. Spitzer, Jr. and R. Härm, Phys. Rev. **76**, 904 (1949).

[1] S.I. Braginskii in Reviews of Plasma Physics (Consultants Bureau, NY, 1965) Vol. 1, p. 205.

[1] M. N. Rosenbluth and A. N. Kaufman, Phys. Rev. 109, 1 (1958).

[1] W. Gekelman, H. Pfister, Z. Lucky, J. Bamber, D. Leneman and J. Maggs, Rev. of Sci. Instrum. **62**, 2875 (1991).

[1] D. D. Needleman and R. L. Stenzel, Phys. Rev. Lett. **58**, 1426 (1987).

[1] J. Bowles, R. McWilliams and N. Rynn, Phys. Rev. Lett. **68**, 1144 (1992).

[1] F. Anderegg, X. P. Huang, C. F. Driscoll, E. M. Hollmann, T. M. O'Neil and D. H. E. Dubin, Phys. Rev. Lett. **78**, 2128 (1997).

[1] I. H. Hutchinson, ‘Principles of Plasma Diagnostics’, pp 95-115, Cambridge University Press, New York, NY (1987).

[1] W. H. Press, S. A. Teukolsky, W. T. Vetterling and B. P. Flannery, ‘Numerical Recipes in C’, second Ed., p 856, Cambridge University Press, New York, NY (1992).

[1]J. E. Maggs and G. J. Morales, Phys. Plasmas **4**, 290 (1997).

References

[1] L. Spitzer, Jr. and R. Härm, Phys. Rev. **76**, 904 (1949).

[2] S.I. Braginskii in Reviews of Plasma Physics (Consultants Bureau, NY, 1965) Vol. 1, p. 205.

[3] M. N. Rosenbluth and A. N. Kaufman, Phys. Rev. 109, 1 (1958).

[4] W. Gekelman, H. Pfister, Z. Lucky, J. Bamber, D. Leneman and J. Maggs, Rev. of Sci. Instrum. **62**, 2875 (1991).

[5] D. D. Needleman and R. L. Stenzel, Phys. Rev. Lett. **58**, 1426 (1987).

[6] J. Bowles, R. McWilliams and N. Rynn, Phys. Rev. Lett. **68**, 1144 (1992).

[7] F. Anderegg, X. P. Huang, C. F. Driscoll, E. M. Hollmann, T. M. O’Neil and D. H. E. Dubin, Phys. Rev. Lett. **78**, 2128 (1997).

[8] I. H. Hutchinson, ‘Principles of Plasma Diagnostics’, pp 95-115, Cambridge University Press, New York, NY (1987).

[9] W. H. Press, S. A. Teukolsky, W. T. Vetterling and B. P. Flannery, 'Numerical Recipes in C', second Ed., p 856, Cambridge University Press, New York, NY (1992).

[10] J. E. Maggs and G. J. Morales, Phys. Plasmas **4**, 290 (1997).